

Carbon K -edge fine structure in graphite foils and in thin-film contaminants on metal surfaces

D. Denley,* P. Perfetti,[†] R. S. Williams,[‡] and D. A. Shirley

Materials and Molecular Research Division, Lawrence Berkeley Laboratory, Berkeley, California 94720
and Department of Chemistry, University of California, Berkeley, California 94720

J. Stöhr

Stanford Synchrotron Radiation Laboratory, Stanford, California 94305

(Received 10 August 1979)

We report absorption and extended-fine-structure studies on the carbon K edge in microcrystalline, polycrystalline, and oriented crystalline (monochromator) graphite. On the basis of a density-of-states analysis, strong excitonic effects about the core hole are inferred. The fine structure at the absorption edge is found to differ for the three materials. This is explained by the orientational dependence of the polarization selection rules for electric dipole transitions from an s core to σ and π conduction-band states. The extended x-ray fine structure (EXAFS) above the edge exhibits similar oscillations for the bulk crystalline samples (polycrystalline and monochromator graphite), but considerably weaker structure is observed for the microcrystalline sample. A Fourier analysis of the oscillations yields the nearest-neighbor shell separations. Finally, it is shown that the intensity modulations caused by carbon contamination on optical Au and Pt mirror surfaces that are exposed to high-intensity synchrotron radiation closely resemble those above the C K edge in bulk crystalline graphite. This indicates the formation of graphitic overlayers on such mirrors even under ultrahigh-vacuum ($< 1 \times 10^{-9}$ Torr) conditions. These findings furthermore demonstrate the feasibility of EXAFS studies of adsorbates on surfaces by monitoring the (totally) reflected radiation off the substrate.

I. INTRODUCTION

Measurements from core-level excitations in solids can provide information that is otherwise difficult to obtain. In the initial ~ 50 eV above the onset for absorption from a core-level, initial-state band effects dominate the absorption so that the spectra yield information on the electronic structure of the material immediately above the Fermi level. The effect of the optical-dipole selection rules is to cause spectra to represent a symmetry-projected density of states, since the initial state is of good angular momentum. This was demonstrated for absorption from the K edge in the $4d$ transition metals by Müller *et al.*¹ In some cases many-body effects,^{2,3} low cross section due to final-state effects,⁴ and multiplet splitting⁵ can interfere with simple interpretations.

For higher final-state energies the remaining features arise mainly from the local arrangement of atoms in the material.⁶ This extended x-ray absorption fine structure (EXAFS) has proved valuable for structural analysis in the moderate x-ray energy regime 3–25 keV, but only recently have absorption measurements been made on the important low- Z elements C (Refs. 7 and 8) and F (Ref. 8). In addition, C (Ref. 9), N (Ref. 10), and O (Refs. 10 and 11) have been studied by the related techniques of electron energy loss and photo yield spectroscopy.

In this paper we report the first absorption measurements taken above the carbon K edge in a series of graphite samples. Figure 1(a) shows the graphite lattice. The lattice translation vectors \vec{a} and \vec{b} lie in the basal plane, while the vector \vec{c} represents translation perpendicular to the plane. The Brillouin zone is a right hexagonal prism, shown in Fig. 1(b) with the symmetry points labeled.

In Sec. II the experiments are described. Results are given in Sec. III. Section IV is devoted to a discussion of the absorption in the band-structure (near-edge) region and the morphology (extended-edge) data. Section V reports our observation of EXAFS structure in reflection from thin

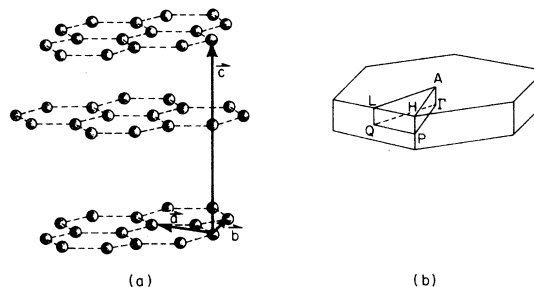


FIG. 1. Structure of graphite (a) in real space showing the crystal translation vectors and (b) reciprocal space Brillouin zone with the labels of the symmetry points.

films contaminating metal surfaces. Conclusions are given in Sec. VI.

II. EXPERIMENTAL

The experiments were performed on the 4° port¹² of Beam Line I at the Stanford Synchrotron Radiation Laboratory (SSRL). Before the measurements were made, new optical elements were installed to minimize carbon buildup on the optical surfaces of the grazing incidence "grasshopper" monochromator¹² that occurs on exposure to high fluxes of synchrotron radiation.¹³ These included a new 600 lines/mm grating blazed to 220 eV. At the time of these measurements the bandpass of the monochromator was 0.2 Å, and measurements of the monochromator transmission indicated the presence of monochromatic radiation up to at least 1400 eV. The experimental apparatus has been described in detail elsewhere.^{14,15}

Because of the vacuum restriction of the radiation source and the short photon attenuation lengths in the soft x-ray photon energy regime, the sample and detector were maintained in an ultrahigh-vacuum environment of 3×10^{-9} for these experiments. The radiation first passed through a collimator to define the beam and eliminate scattered-light background. Next, the light struck the sample holder on which samples and reference blanks were arranged in alternate positions. A microprocessor-controller drove a stepping motor-and-cam arrangement that allowed the sample and the reference blank to intercept the beam before advancing the monochromator, thus allowing the immediate calculation of the optical density $\ln(I_0/I)$. The remaining radiation was detected by a ZnS or Au photocathode. The resulting photoelectrons were extracted by a bias voltage to a high-current channeltron electron multiplier. This overall detection scheme yielded a good signal level (10^{-5} – 10^{-7} A) with a low background ($<10^{-11}$ A). By selecting the optimal photocathode material for the particular photon energy range of interest, the ratio of first-order to second-order light from the monochromator could be enhanced.

The absorption spectra were taken for three graphitic samples: evaporated carbon foils¹⁶ with a thickness approximately 50 mg/cm² (2500 Å), evaporated carbon foils that were subsequently annealed in vacuum for three minutes at 1100 °C, and a thin sample cleaved from a crystal of stress-annealed monochromator graphite.¹⁷ The three samples differ in crystallite size and orientation. The evaporated foils generally have a crystalline size of ~10–15 Å and no discernible orientation.¹⁸ For the purposes of our discussion, they will be referred to as *microcrystalline*. The foils that were subsequently annealed have a cry-

stallite size of ~2500 Å as determined by transmission electron microscopy, and are known to show preferential ordering with the *c* axis becoming normal to the surface plane.¹⁹ These samples will be referred to as *polycrystalline*. The monochromator graphite is a well-ordered mosaic of crystallites, with the basal planes parallel to the surface plane. While the \vec{a} and \vec{b} in-plane crystal axes do not maintain their rotational orientation about the \vec{c} direction throughout the sample, monochromator graphite is otherwise quite similar to single-crystal graphite.²⁰

III. RESULTS

Spectra near the carbon *K* edge are displayed in Fig. 2, and energies of characteristic features A–I are set out in Table I. Features in the polycrystalline and monochromator graphite spectra show a one-to-one correspondence, the edge jump ratio is much smaller in the monochromator graphite case, and absorption above the edge shows nearly zero overall slope. This results from nonuniformities in the thickness of the monochromator graphite, which we were unable to eliminate for a sample of the required dimensions (~5-mm diameter). There are also differences between the microcrystalline sample and the other two. For this sample, all the features are weakened or broadened, as might be expected in a highly disordered system. In the extended region, the features E and I, which are higher-frequency compo-

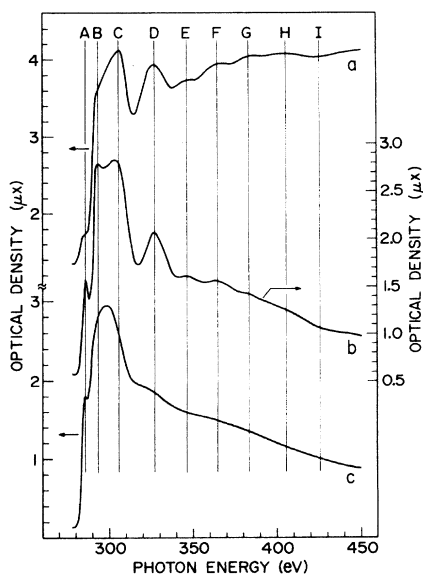


FIG. 2. Absorption spectra for graphite in the (top) monochromator, (middle) polycrystalline, and (bottom) microcrystalline forms. The optical density μx is the product of the absorption coefficient μ and distance x . $I = I_0 e^{-\mu x}$.

TABLE I. Comparison of carbon K -edge absorption to electron-loss (ELS) and secondary-electron emission (SEE) measurements and to the calculated density of states (DOS).

Feature	Absorption (eV)	ELS (eV)	SEE ^a (eV)	Calculated DOS (eV)
A	285	285		2.0
B	293	293	9.5	9.9
C	302	304	19.2	18.3
D	325	325	40.7	42.0
E	344			
F	362	356		
G	381	380		
H	403	400		
I	423	422		

^aThe SEE results and the calculated density of states should be compared by adding the threshold energy (285 eV).

nents of the spectra characteristic of longer-range neighbors, are greatly reduced in amplitude. A more detailed analysis of the EXAFS structure is given below.

IV. NEAR-EDGE REGION AND EXAFS STRUCTURE

The absorption immediately above the edge is shown in Fig. 3. A peak appears at 285 eV in the polycrystalline and microcrystalline samples, and a sharp edge rises to a second peak at 293 eV in the polycrystalline case. For the monochromator sample the first peak is replaced by a low plateau and the sharp edge is rounded at the top, yielding no distinct peak. The intensity of the low-energy peak decreases in the order

(microcrystalline foil) > (polycrystalline foil)
> (monochromator graphite).

We attribute this to a polarization effect arising from the crystalline anisotropy of graphite. The band structure^{21,22} of graphite is quasi-two-dimensional because of the weakness of the interactions

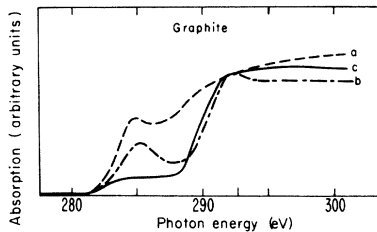


FIG. 3. Near-edge absorption spectra for (a) microcrystalline, (b) polycrystalline, and (c) monochromator graphite showing the polarization effect for the first π band.

between planes, and most dispersive effects occur in the basal-plane directions.

The first states above the Fermi level have the character of π bonds arising from p_x orbitals directed out of the plane. This band starts near E_F where the density of states has a shallow minimum. It has a rather flat saddle point about 2 eV above E_F and at the zone face Q (see Fig. 4). Because the band structure is quasi-two-dimensional, the saddle point should contribute a near-logarithmic Van Hove singularity to the density of states. We therefore assign the peak at 285 eV to transitions to that critical point of π_0 at Q (labeled Q_{2g}^- in Ref. 21) and the second peak at 293 eV to the peak in the density of states calculated to lie at 8.5 eV in Ref. 22. The latter is mainly $sp^2\sigma$ in character and due to the bands labeled σ_1 and σ_2 at Q (Q_{1g}^+ in Ref. 21). From the band symmetries, transitions from the $1s$ core level to the σ bands are forbidden for the light polarization vector $\vec{\epsilon}$ parallel to \vec{c} , and transitions to the π bands are forbidden for $\vec{\epsilon} \perp \vec{c}$. Our results are explained by noting that, as the c axis of the crystallites becomes progressively more aligned with the foil surface plane, the $1s \rightarrow \sigma$ transition remains allowed, while the $1s \rightarrow \pi$ transition becomes forbidden.

The separation of the first and second peaks (8 eV) is 1–3 eV larger than is calculated.²² This effect can be explained by comparison with the x-ray photoemission (XPS) measurements of the carbon- $1s$ binding energy.²³ Because the measured binding energy is 284.7 eV, the saddle point at Q would not be expected below 287 eV in a simple one-electron picture. Relaxation effects arising from the attraction of the low-energy electron to the core

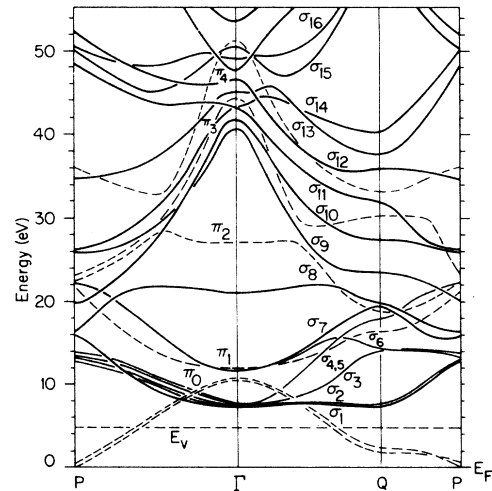


FIG. 4. Band scheme for graphite, after Ref. 22. The bands are labeled as to π or σ character.

hole must account for the 2 eV shift of the π peak. A rigid shift of the density of states above the Fermi level would place the absorption onset at approximately 283 eV and indicate the formation of bound excitonic states in graphite, although a complete distortion of the density of states is possible. The very recent high-resolution electron-loss (ELS) results of Mele and Ritsko²⁴ indicate that such a distortion is probably correct—the observed onset in their data is no more than 0.2 eV below the carbon-1s binding energy and a model calculation gives a good fit to the distortion in the density of states at the π peak.

For Peak B and all those at higher energies, our results can also be compared to the secondary-electron emission (SEE) spectra reported by Willis, Fitton, and Painter²² (see Table I). In addition, one feature (peak D) has been observed in a photoemission study.²⁵ Peak B in Fig. 2, at 293 eV, corresponds well to a feature reported in the SEE measurements at 9 eV above the Fermi level (i.e., at 29 eV) as well as to the peak at 292 eV in the ELS spectrum. Peak C has no analog in the ELS spectrum, but it does correspond to a feature at 19.2 eV in the SEE results and a peak in the calculated density of states due mainly to critical points in the σ bands at Q . All three results show that there is a broad peak at 41 eV above E_F where the theoretical calculation predicts a broad peak due mainly to σ bands.

There is an important by-product of this observation. Peak D occurs at $E_F + 40$ eV, on the threshold of the conventional extended-x-ray-absorption (EXAFS) regime, and might ordinarily be included in the EXAFS analysis. In fact, Peak D probably arises at least in part from simple structural effects, as evidenced by the continued presence of this feature in a weakened form in the ELS results for which the geometry forbids transitions to σ bands. Of course, band-structure effects do not preclude obtaining structural information if they are properly accounted for. However, if the final-state energy is high enough (at least above Peak C), detailed band-structure effects become less important and the single-scattering theory generally holds,^{6,26} in which it is sufficient to treat the solid as a collection of atomic potentials. In this case, the relation

$$\frac{\mu - \mu_0}{\mu_0} = \chi(k) = \frac{1}{k} \sum_j \frac{N_j}{R_j^2} A(k) \sin[2kR_j + \phi(k)] \times \exp(-2\sigma^2 k^2 - 2R_j/\lambda) \quad (1)$$

describes the EXAFS oscillations $\chi(k)$ that occur about a slowly varying absorption μ_0 . The electron wave vector is given by

$$k = 0.5123(\hbar\omega - E_0 + E_i)^{1/2} \text{ \AA}^{-1}, \quad (2)$$

with energies expressed in eV, where the onset of absorption E_0 and the inner potential E_i set the zero of electron kinetic energy. The sum is taken over shells of j th neighbor atoms consisting of N_j atoms at a distance R_j from a central atom. The backscattering strength is $A(k)$, and ϕ is the total energy-dependent phase shift that an electron experiences upon returning to the central site after backscattering. Thermal oscillations from the equilibrium lattice positions are described by σ , and λ is the mean electron attenuation length.

In general, a radial distribution function can be deduced from the EXAFS data if the effects of phase shifts due to the atomic potentials are compensated. Figures 5 and 6 give plots of the radial distribution function

$$R(r) = |F(r)| = \left| \int dr \frac{e^{-i\phi(k)}}{A(k)} k\chi(k) \right|$$

for polycrystalline and monochromator graphite. The backscattering amplitude²⁷ and the phase shift²⁸ are taken from calculated values. As in the work of Lee and Beni,²⁶ the inner potential E_i is adjusted until the peaks in $R(r)$ and $\text{Im}F(r)$ coincide. The best results were obtained in polycrystalline graphite with E_i set 24 eV above the absorption threshold and 19 eV in monochromator graphite. Both curves show residual amplitude near $r=0$. This is an artifact arising from the limited data range, causing the degree of noncancellation between positive and negative excursions to become serious. The problem is aggravated by the short bond length in graphite.

Table II gives the distances of the different shells in the graphite lattice, together with the number of atoms in each shell. The quality factor $Q = N_j R_1^2 / R_j^2$ serves as a rough measure of the expected weight of a given shell; Q neglects polarization effects, which can be important for oriented samples.²⁹

The results for $R(r)$ in polycrystalline graphite show a main peak at 1.41 ± 0.04 \AA and three smaller peaks of similar strength above the main peak at 2.54, 3.84, and 4.90 \AA. The first peak corre-

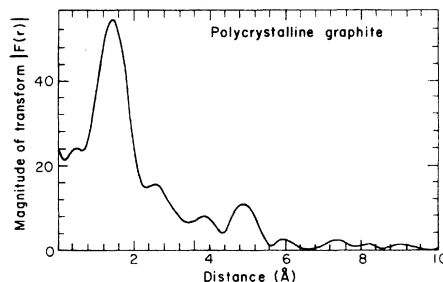


FIG. 5. Radial distribution function from the polycrystalline graphite EXAFS data.

sponds quite well to the first-nearest-neighbor (NN) distance in graphite. The second is clearly a weighted mean of the second and third NN in the basal plane. At higher distances the neighbors on the first "neighbor plane" (NPNN) to the basal plane containing the central atom begin to occur in addition to the in-plane nearest neighbors (IPNN). The third peak is expected to be a mean of the fourth through ninth NN, which form a fairly separate grouping of two IPNN and four NPNN. The (unknown) weighting between these two classes of neighbors is dependent upon the degree of crystalline orientation, although the polarization effect between the in-plane and nearest-plane neighbors will be less significant for distances greater than ~ 4.7 Å. The final peak may contain components from as far as the thirteenth NN.

The radial distribution function for monochromator graphite is shown in Fig. 6. In this case, a somewhat shorter data set was obtained, which resulted in poorer resolution. Nonetheless, the first NN peak (1.39 ± 0.06 Å) is obvious and there is a second peak at 3.36 Å which may result from a combination of the second through the ninth NN. In fact, the peak occurs at a value intermediate between a mean weighted simply by the factor Q in Table II and one neglecting the NPNN altogether. However, the deep minimum between the first and second peaks gives clear evidence of interference of the higher neighbors with the broadened peak from the first NN, which makes further interpretation difficult.

In the microcrystalline spectrum (Fig. 2) two effects appear. All features are considerably lower in amplitude and from the disappearance of peaks E and H together with the removal of the minima between F and G, it is clear that the higher spatial frequencies are no longer present. In fact, a plot of the remaining maxima and minima in the remaining features clearly suggests that the first NN is virtually the only remaining component.

V. EXAFS IN REFLECTION (REXAFS)

One obstacle to making structural measurements from the carbon K edge is the proximity of absorption edges of other common materials. In particular, O- $1s$ (532 eV) and Ti- $2p$ (455 eV) contamination can be troublesome. Another is the degradation of the reflecting elements of monochromators above 280 eV due to carbon contamination. The resulting loss of intensity is obvious in the plot of monochromator throughput (Fig. 7).

A blowup of the monochromator output (Fig. 8) merits discussion. The inverted figure shows fine structure for at least 100 eV above threshold

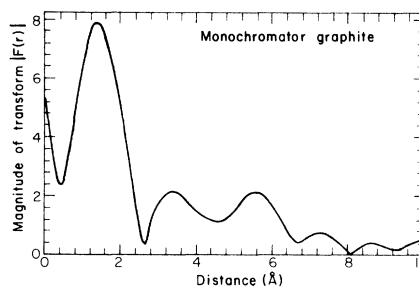


FIG. 6. Radial distribution function from the monochromator graphite EXAFS data.

and compares feature for feature with the polycrystalline graphite absorption spectrum. What is being observed here is EXAFS from the carbon contamination of the optical elements in reflection (REXAFS). In fact, from the considerable correspondence of the REXAFS with the polycrystalline and monochromator graphite EXAFS, we conclude that the carbon contamination common to soft x-ray monochromators and other surfaces of accelerators may be a well-ordered graphitic material. We have no measure of the background signal that was present, so we can only estimate a lower limit to the thickness of the total carbon layer on the five reflecting surfaces as 25 Å. It seems possible, then, that EXAFS measurements in the reflection mode can serve as a surface-analytical tool for adsorbate systems. Although the technique may be more sensitive to bulk contaminants than the more common low-energy electron spectroscopies due to the longer absorption lengths of soft-x-ray photons, this effect can be

TABLE II. Parameters for neighbor shells of atoms in graphite.

Neighbor ^a j	Occupancy of shell N_j	Quality ^b factor Q	Distance R_j (Å)
1	3	3.0	1.421
2	6	2.0	2.461
3	3	0.75	2.842
4 ^a	1	0.18	3.354
5 ^a	9	1.37	3.642
6	6	0.86	3.750
7 ^a	6	0.70	4.160
8	6	0.50	4.263
9 ^a	9	0.94	4.396
10	6	0.50	4.922
11 ^a	18	1.43	5.038
12	6	0.46	5.123
13 ^a	6	0.41	5.424
14	3	0.19	5.684

^a Entries indicate out-of-plane neighbor shells.

^b $N_{\text{shell}}(R_1/R_{\text{shell}})^2$; $R_1 = 1.421$.

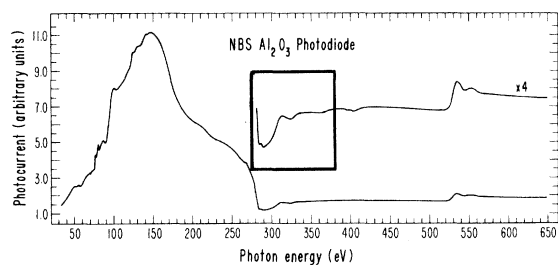


FIG. 7. Monochromator transmission measurement from the 4° line grasshopper monochromator as measured by an NBS calibrated photodiode. At the time of the measurement, the optical surfaces had been exposed to synchrotron radiation for approximately two years. The region above the carbon *K* edge is expanded and the boxed portion is reproduced in Fig. 8.

minimized by going to grazing angles of incidence.

A rough estimate of the magnitude of the effect can be made by modeling the adsorbate system (e.g., a monolayer of CO on platinum or gold) by a thin dielectric layer of one monolayer depth on a thick substrate. One can then calculate the reflectivity³⁰ for the surface with (R_{ads}) and without (R_0) the monolayer-thick dielectric film from published values.³¹ A plot of the differential reflectivity $(R_0 - R_{\text{ads}})/R_0$ in Fig. 9 shows two effects. There is a jump at the threshold of $\sim 5\%$ that is comparable to the results of either Auger³² or yield¹⁰ electron spectroscopies for monolayer adsorbate systems, and the function $(R_0 - R_{\text{ads}})/R_0$ does image the features that would be expected in absorption.

VI. CONCLUSIONS

The results obtained on the C *K* edge in graphite fall into two groups. In the first 40 eV of absorption, information is obtained regarding the $l=1$ projected density of states. Good agreement was found with the structure in electron energy loss⁹ and secondary-electron emission²² although not all features found were represented in our spectra, with most of the differences ascribable to polarization effects. In addition to providing support for the predicted band structure, it confirms the reorientation of the microstructure¹⁹ as reported previously. Band-structure effects were found to be quite strong for over 40 eV above the absorption threshold.

The remaining features at higher energies were found to yield good structural information in graphite by application of simple single-scattering EXAFS theory. The annealed (polycrystalline) sample was found quite similar to monochromator graphite and neighbor shells out to $\sim 5 \text{ \AA}$ were measured. The microcrystalline sample shows a

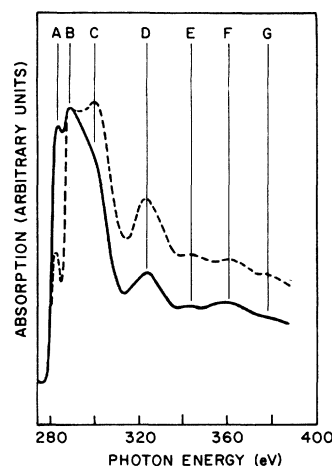


FIG. 8. Portion of the transmission function from Fig. 7 is inverted (full line) as compared to the absorption spectrum of the polycrystalline graphite foil (dashed line). All features of the graphite spectrum are found in the monochromator transmission function.

large attenuation for all shell distances beyond the first, which presumably results from short-range disorder.

We have observed and analyzed EXAFS oscillations in reflection (REXAFS) for the first time from the contaminant layers that plague soft-x-ray and particle accelerator equipment and determined it to be graphitic in nature. This observation

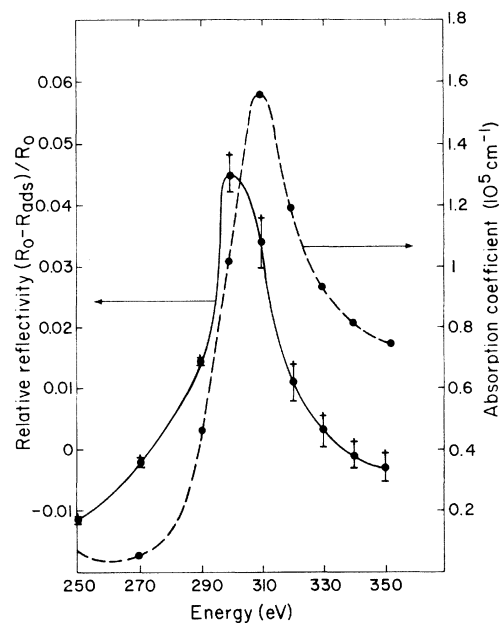


FIG. 9. Absorption coefficient for carbon (dashed lines) from Ref. 29, and relative reflectivity $(R_0 - R_{\text{ads}})/R_0$ (solid line). Also included as bars on the data are calculations for which the absorption coefficient of the overlayer has been modulated by $\pm 10\%$.

should be useful in future attempts at improving such equipment.

ACKNOWLEDGMENT

This work was supported by the Division of Chemical Sciences, Office of Basic Energy Sci-

ences, U.S. Department of Energy under Contract No. W-7405-Eng-48. It was performed at the Stanford Synchrotron Radiation Laboratory, which is supported by the NSF under Grant No. DMR 77-27489, in cooperation with the Stanford Linear Accelerator Center.

*Also with the Department of Physics, University of California, Berkeley.

†Permanent address: Laboratori Nazionale di Frascati (PULS), Casella Postale 13, 00044 Frascati, Roma, Italy.

‡Permanent address: Bell Laboratories, Murray Hill, New Jersey.

¹J. E. Müller, O. Jepsen, O. K. Anderson, J. W. Wilkins, *Phys. Rev. Lett.* **40**, 720 (1978).

²G. D. Mahan, *Phys. Rev.* **163**, 612 (1967).

³P. Nozières and C. T. DeDominicis, *Phys. Rev.* **178**, 1097 (1969).

⁴W. Gudat, C. Kunz, and J. Karlan, *Appl. Opt.* **13**, 1412 (1974).

⁵J. Sugar, *Phys. Rev. B* **5**, 1785 (1972).

⁶F. W. Lytle, D. E. Sayers, and E. A. Stern, *Phys. Rev. B* **15**, 2426 (1977).

⁷F. C. Brown, R. Z. Bachrach, A. Bianconi, *Chem. Phys. Lett.* **54**, 425 (1978).

⁸R. S. Williams, D. Denley, D. A. Shirley, and J. Stöhr (unpublished).

⁹B. M. Kincaid, A. E. Meixner, and P. M. Platzman, *Phys. Rev. Lett.* **40**, 1296 (1978).

¹⁰J. Stöhr, *J. Vac. Sci. Technol.* **16**, 37 (1979).

¹¹J. Stöhr, D. Denley, and P. Perfetti, *Phys. Rev. B* **18**, 4132 (1978).

¹²F. C. Brown, R. Z. Bachrach, S. B. M. Hagström, N. Lien, and C. H. Pruett, *Vacuum Ultraviolet Radiation Physics*, edited by E. E. Koch, R. Haensel, and C. Kunz (Pergamon, Viewig, 1974), p. 785.

¹³D. A. Shirley, *Workshop on x-ray Instrumentation for Synchrotron Radiation Research*, edited by H. Winick and G. Brown (Stanford Synchrotron Radiation Laboratory Report No. 78/04), p. VII-80 (unpublished).

¹⁴D. Denley, R. S. Williams, P. Perfetti, D. A. Shirley, and J. Stöhr, *Phys. Rev. B* **19**, 1962 (1979).

¹⁵J. Stöhr and D. Denley, in Ref. 13, p. VIII-181.

¹⁶The evaporated carbon foils were obtained from the Arizona Carbon Foil Company, Tucson, Arizona.

¹⁷A "ZYA"-grade monochromator was obtained from the Union Carbide Corporation and cleaved with scotch tape.

¹⁸G. M. Jenkin, J. A. Turnbull, and G. K. Williamson, *J. Nucl. Mater.* **7**, 215 (1962).

¹⁹T. Evans and P. F. James, *Proc. R. Soc. London A277*, 260 (1964).

²⁰A. W. Moore in *Chemistry and Physics of Carbon*, edited by P. L. Walker and P. A. Thrower (Dekker, New York, 1973).

²¹G. S. Painter and D. E. Ellis, *Phys. Rev. B* **1**, 4747 (1970).

²²R. F. Willis, B. Fitton, and G. S. Painter, *Phys. Rev. B* **9**, 1926 (1974).

²³F. R. McFeely, S. P. Kowalczyk, L. Ley, R. G. Cavell, R. A. Pollak, and D. A. Shirley, *Phys. Rev. B* **9**, 5268 (1974).

²⁴E. J. Mele and J. J. Ritsko, *Phys. Rev. Lett.* **43**, 68 (1979).

²⁵A. Bianconi, S. B. M. Hagström, and R. Z. Bachrach, *Phys. Rev. B* **16**, 5543 (1977).

²⁶P. A. Lee and G. Beni, *Phys. Rev. B* **15**, 2862 (1978).

²⁷B.-K. Teo, P. A. Lee, A. L. Simmons, P. Eisenberger, and B. M. Kincaid, *J. Am. Chem. Soc.* **99**, 384 (1977).

²⁸P. A. Lee, B.-K. Teo, and A. L. Simons, *J. Am. Chem. Soc.* **99**, 3856 (1977); B.-K. Teo and P. A. Lee (private communication).

²⁹S. M. Heald and E. A. Stern, *Phys. Rev. B* **16**, 5549 (1977).

³⁰A. N. Bloch and S. A. Rice, *Phys. Rev.* **185**, 933 (1969).

³¹H.-J. Hagemann, W. Gudat, and C. Kunz, DESY Report No. SR-74/7, 1974 (unpublished).

³²P. H. Citrin, P. Eisenberger, and R. H. Hewitt, *Phys. Rev. Lett.* **41**, 309 (1978).